Supplement Material

Supplemental Figure I, Castranova et al.

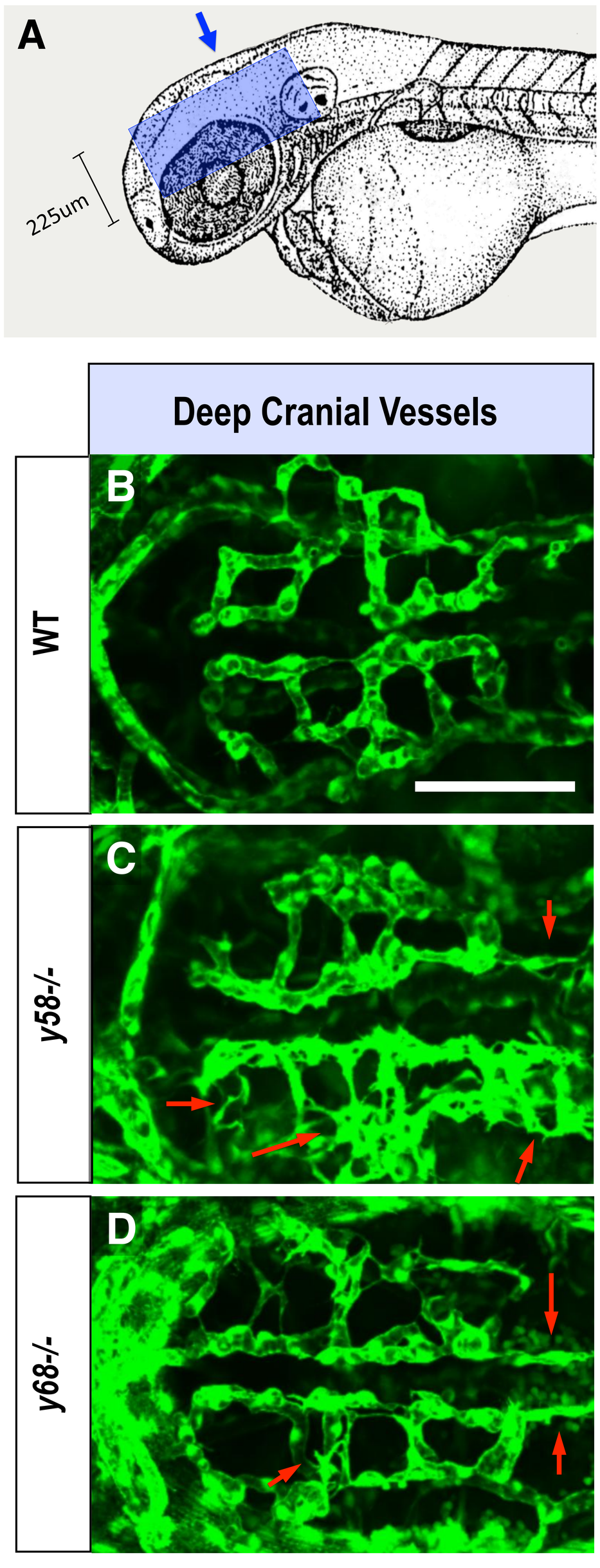

S Fig I. Zebrafish *y58* and *y68* mutants display excess angiogenesis in deep cranial vessels. (A) Schematic diagram of a 2 dpf zebrafish head (modified from (22)), with a blue box showing the approximate position of images in B-D. **(B-D)** Confocal fluorescence micrographs of the cranial vasculature (with dorsal most cranial vessels omitted) of 2 dpf *Tg(fli1a-EGFP)^{y1}* transgenic wild type sibling (B), *Tg(fli1a-EGFP)^{y1} y58* mutant (C), and *Tg(fli1a-EGFP)^{y1} y68* mutant (D) animals. Dorsal views, rostral to the left. Arrows in C, and D note ectopic vessel branches observed in *y58* and *y68* mutant animals. Scale bar = 100 µm (B).

Supplemental Figure II, Castranova et al.

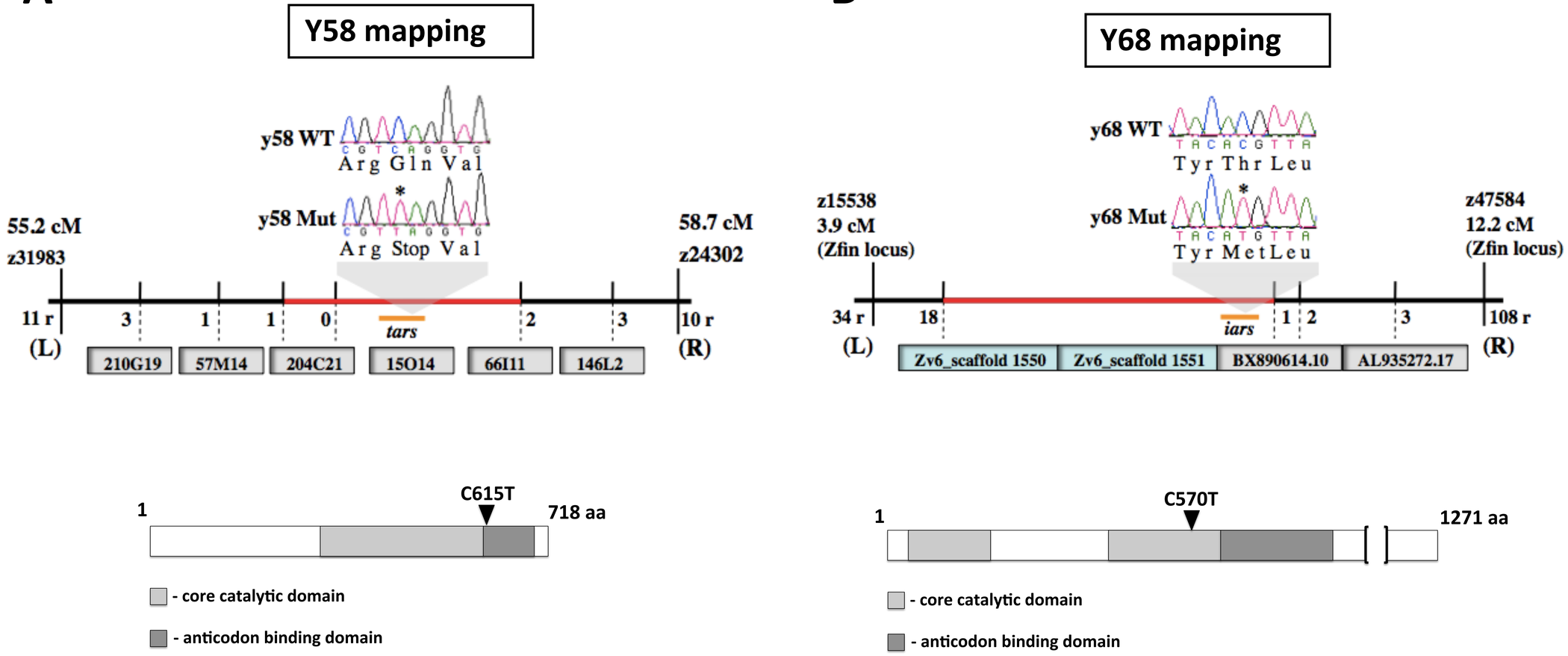

S Fig II. Mapping and positional cloning of the *y58* and *y68* mutants. (A) Mapping and positional cloning of *y58,* revealing a mutation in the *threonyl tRNA synthetase (tars)* gene resulting in early termination of the polypeptide sequence prior to the anticodon binding domain of the enzyme. **(B)** Mapping and positional cloning of y68, revealing a mutation in the *isoleucyl tRNA synthetase (iars)* gene changing a conserved threonine in the core catalytic domain to a methionine.

Supplemental Figure III, Castranova et al.

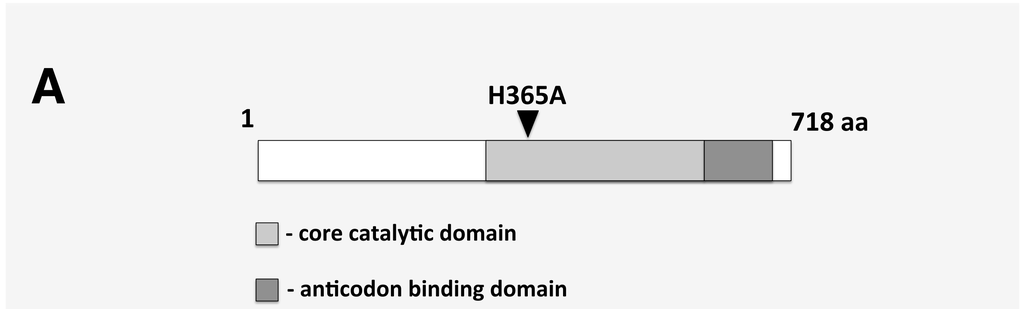

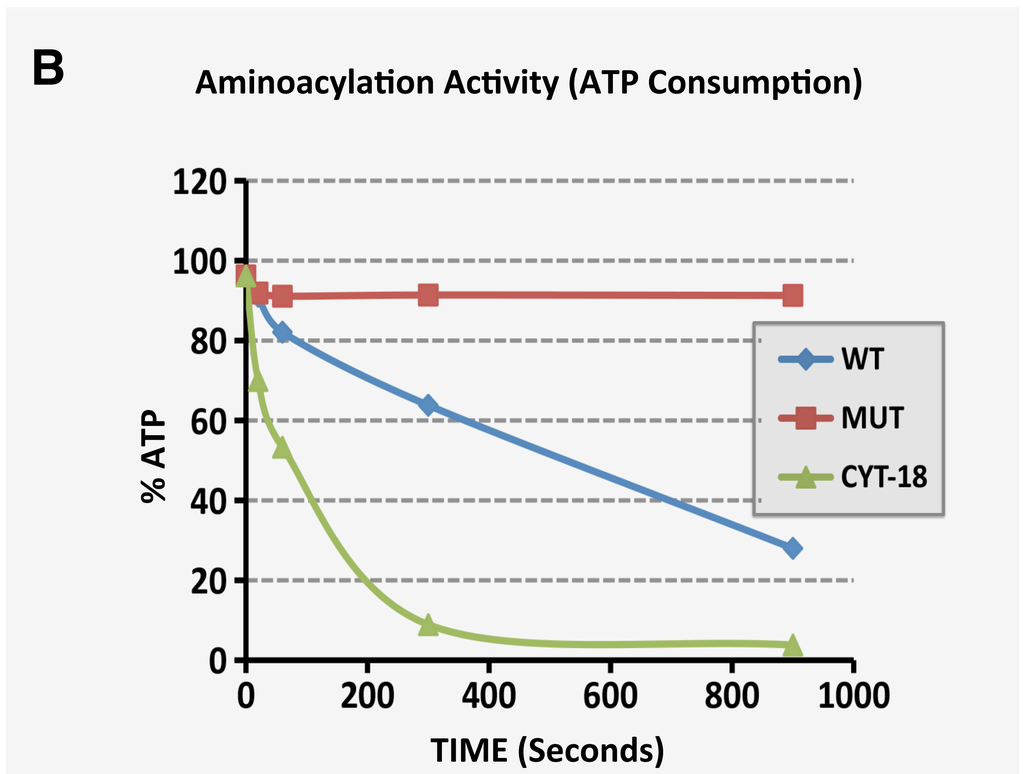

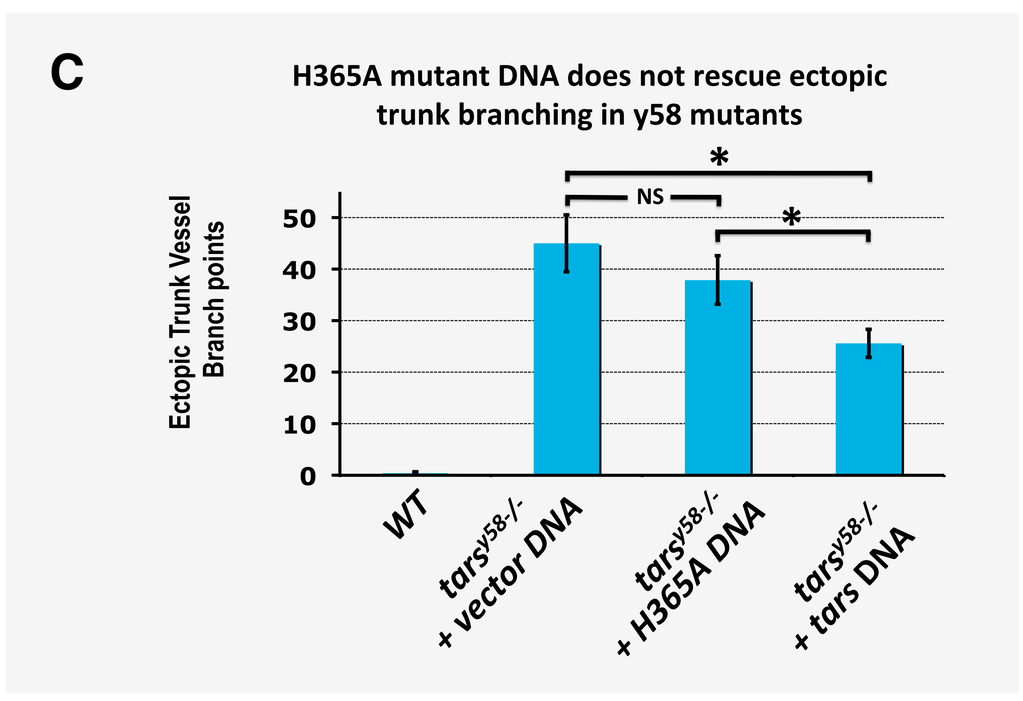

S Fig III. Kinase-dead TARS does not rescue the defects in *tars* mutants. (**A**) Diagram showing *tars* polypeptide and the position of the mutation changing a conserved histidine in the active site to an alanine. (**B**) Graph showing ATP consumption vs. time in an *in vitro* aminoacylation assay using purified zebrafish wild type tars and mutant tars(H365A) protein, with purified N. crassa Tyrosyl RNA synthetase (CYT-18) as a positive control. **(C)** Quantitation of the number of ectopic trunk intersegmental vessel branch points observed in phenotypically wild type (WT) siblings (Column 1, N = 10), *Tol2(beta-actin:mCherry)*-injected $tars^{y58-/-}$ mutants (Column 2, N = 9), *Tol2(beta-actin:*$tars^{H365A}$*-2A-mCherry)*-injected $tars^{y58-/-}$ mutants (Column 3, N = 9), or *Tol2(beta-actin:*$tars^{WT}$*-2A-mCherry)*-injected $tars^{y58-/-}$ mutants (Column 4, N = 10). Significance at $P < 0.05$ is noted with an asterisk in panel C.

Supplemental Figure IV, Castranova et al.

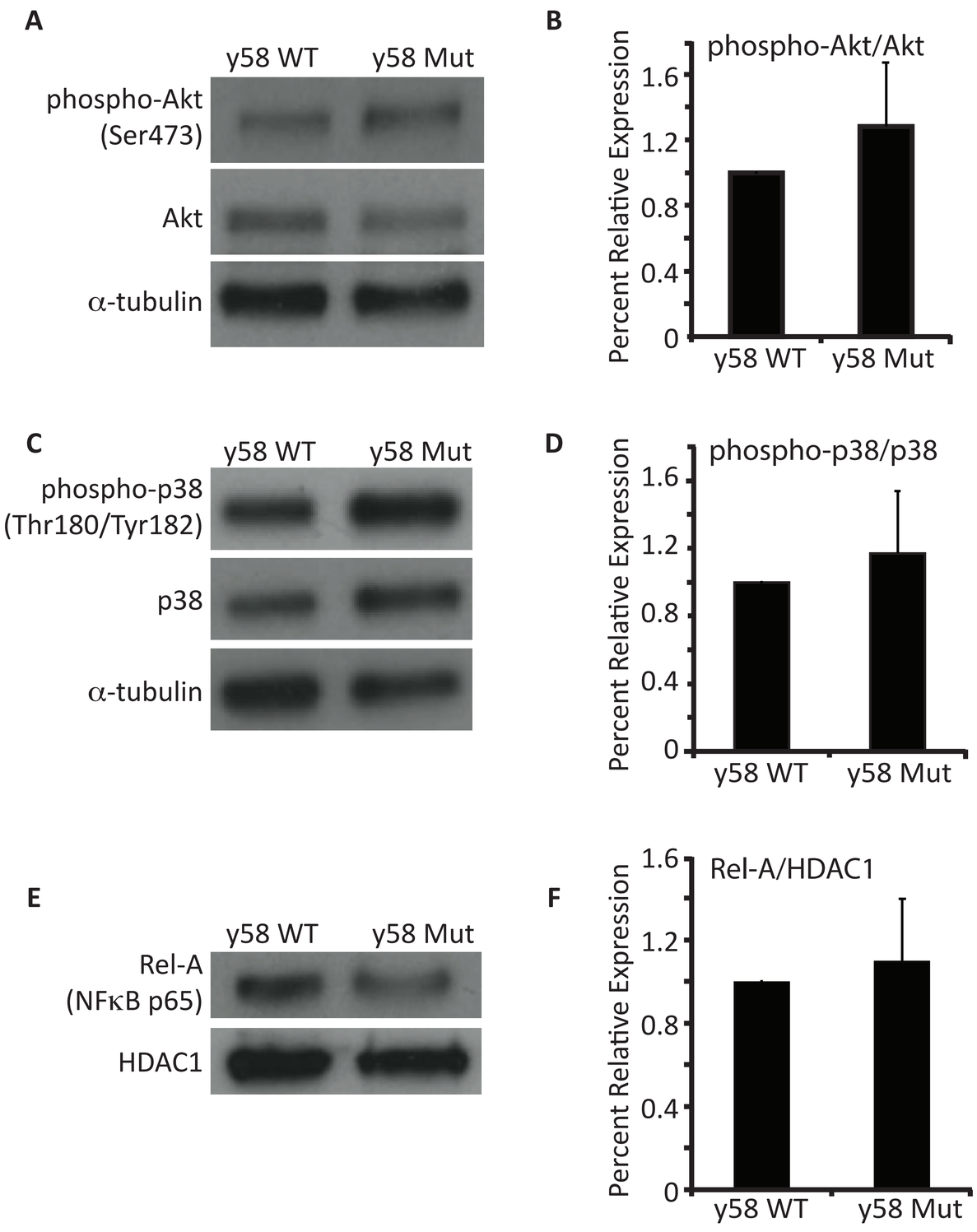

S Fig IV. Western blots assaying potential activation of additional stress pathways. (A-E) (A, C, E) Western blot analysis of downstream components of the PI3K pathway (A), the p38 pathway (C), and the NFκB pathway (E) in y58 mutants and control siblings. (B) Quantification of Akt Western blot, normalizing phospho-Akt expression to total Akt expression. (D) Quantification of p38 Western blot, normalizing phospho-p38 expression to total p38 expression. (F) Quantification of nuclearly expressed Rel-A Western blot, normalizing Rel-A to nuclear loading control, HDAC1.

Supplemental Figure V, Castranova et al.

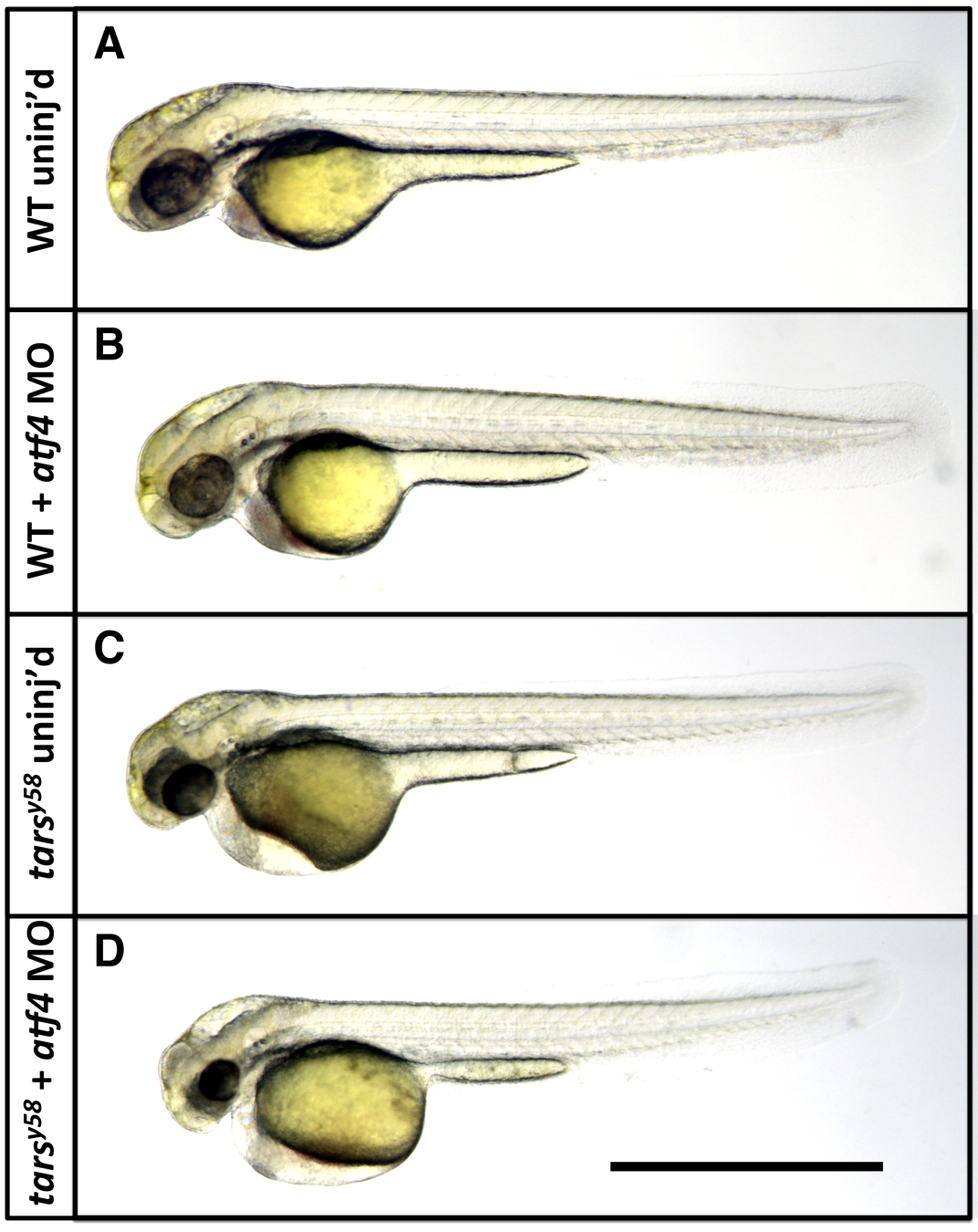

S Fig V. Transmitted light images of wild type sibling and *tars*^{y58} mutant animals with or without atf4 MO injection. (A-D) Transmitted light images of the same animals imaged in Figure 4 panels A-D. 3 dpf wild type sibling (A,C) or *tars*$^{y58-/-}$ mutant (B,D) *Tg(fli1a-EGFP)*^{y1} larvae that were either un-injected (A,B) or injected with 2.5 ng of *atf4* morpholino (C,D). Scale bar = 500 µm.